NJC

PAPER

Cite this: *New J. Chem.*, 2017, **41**, 10000

A reusable multichannel anthraimidazoledione-based receptor for Hg^{2+} and Cu^{2+} ions: ultrasensitive, economical and facile detection of Hg^{2+} in real water sources through fluorescence readout†

Manzoor Ahmad Wani, Neha Thakur, Mrituanjay D. Pandey* and Rampal Pandey *

Received 12th June 2017,
Accepted 3rd August 2017

DOI: 10.1039/c7nj02097j

rsc.li/njc

A reusable multichannel anthraimidazoledione-based receptor **1** has been developed for the highly selective detection of Cu^{2+} and Hg^{2+} in aqueous media. Based on its high fluorescence sensitivity for Hg^{2+}, **1** was probed for the practical detection of Hg^{2+} in various drinking water sources wherein the trace amount of Hg^{2+} was detected through fluorescence 'turn-off' signalling. Hence, **1** revealed qualitative and quantitative practical detection of HTMs (especially Hg^{2+}) in a competitive environment through a multichannel signaling response.

Introduction

The development of multichannel chemosensors for the detection of heavy and transition-metal ions (HTMs) of biological and environmental importance has been an aim of practical research in the recent past.[1] Multichannel chemosensors, signifying a guest binding event through two or more signalling events, such as chromogenic, fluorogenic and electrochemical, are of great importance; however, such receptors are generally scarce.[2] Among various heavy and transition-metal ions (HTM), Cu^{2+} and Hg^{2+} are being widely explored due to their vast influence on the ecosystem and human life. Even at low concentration, mercury (Hg) can cause grave threats to human health, such as loss of vision, renal system failure, prenatal brain injury, DNA impairment and various cognitive and motion disorders.[3] Concerning its toxicity to the environment[4] and fatal effects on health characterized as Minimata disease,[5] the development of Hg^{2+}-selective chemosensors functioning in aqueous medium is essentially important. The World Health Organization (WHO) recommended a limit for inorganic Hg concentration in drinking water of 0.002–0.006 mg L^{-1} (2–6 ppb),[6a] whereas the U.S. Environmental Protection Agency (EPA)-approved Hg limit in drinking water is 2.0 ppb.[6b] Furthermore, 0.5 ppb concentration of Hg can destroy neurite membrane structures.[6c] Therefore, enormous recent interest has arisen toward the practical determination of Hg^{2+} in various real water sources, and there is a continuous need to establish facile, economic and ultrasensitive chemosensors for such practical applications.[7]

Copper (Cu) is an essential trace element involved in metabolic functions performed by the brain, liver, muscles and bones.[8] In coordination with several enzymes, copper, as a cofactor, plays a role in biological electron transport, oxygen transport and neurotransmitter synthesis.[9] Deficiency of Cu in the body can cause impaired immune function, weakened vasculature, abnormal cartilage growth, brain dysfunction and Menkes disease,[10–12] whereas excessive Cu leads to Wilson's disease, Alzheimer's disease, prion disease, kidney failure, gastrointestinal dysfunction and oxidative stress.[13] Therefore, simple and precise methodology for the qualitative and quantitative determination of Hg and Cu in environmental and biological samples is highly sought.[14,15] In this context, designing chemosensors appended with both a fluorophore and a redox-active group has gained attention in the field of molecular recognition because such systems screen out the analyte binding through multichannel signaling.[16] In this context, appending the phenyl-benzimidazole fluorophore with the quinone redox-active group can produce a promising fluorophore–redox conjugate chemosensor.

Through the above perceptions and our continuous work on developing chemosensors,[17] we report herein the synthesis, characterization, crystal structure and multichannel chemosensing behavior of a highly planar redox-active anthraimidazoledione receptor **1** for Cu^{2+} and Hg^{2+}. It is comprised of a benzimidazole

Department of Chemistry, Dr. Harisingh Gour Central University, Sagar, MP, India. E-mail: rppandeysu@gmail.com, mrituanjaypandey@gmail.com

† Electronic supplementary information (ESI) available. CCDC 1501310. For ESI and crystallographic data in CIF or other electronic format see DOI: 10.1039/c7nj02097j

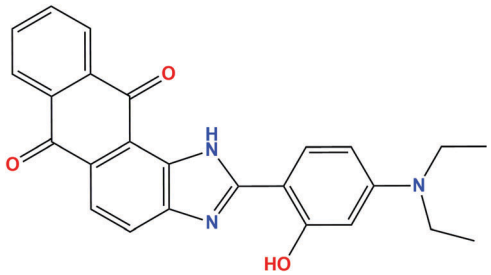

Fig. 1 Chemical structure showing the presence of H-bonding interactions in receptor **1**.

fluorophore and redox-active benzoquinone group to serve as a multichannel chemosensor (Fig. 1). Receptor **1** is functionalized with a couple of N^O chelating sites, thereby involving proficient interaction with metal ions. Besides, **1** contains highly extended π-conjugation; consequently, the overall structure is highly planar, which enables it to exhibit good photophysical properties as well as to act as a fluorescent sensor.[18] Receptor **1** showed naked-eye-visible calorimetric changes for Cu^{2+} and Hg^{2+}, highly sensitive and selective fluorogenic response towards Hg^{2+} ion in aqueous conditions, and electrochemical sensing for Cu^{2+} and Hg^{2+}.[19]

Experimental section

Reagents

To perform the experiment, we used analytical grade reagents, which were first dried and then distilled by usual procedures prior to use.[20] Solvents such as distilled water, absolute ethanol, diethyl ether, and dichloromethane were obtained from HiMedia Chemicals Ltd. The reagents 1,2-diaminoanthraquinone and 4-diethylaminosalicylaldehyde were procured from Sigma-Aldrich Pvt. Ltd. Metal nitrates such as $NaNO_3$, $Ca(NO_3)_2{\cdot}4H_2O$, KNO_3, $Mg(NO_3)_2{\cdot}6H_2O$, $Mn(NO_3)_2{\cdot}4H_2O$, $Fe(NO_3)_2{\cdot}9H_2O$, $Co(NO_3)_2{\cdot}6H_2O$, $Cu(NO_3)_2{\cdot}3H_2O$, $Ni(NO_3)_2{\cdot}6H_2O$, $Cd(NO_3)_2{\cdot}4H_2O$, $Zn(NO_3)_2{\cdot}6H_2O$, $AgNO_3$, $Pb(NO_3)_2$ and $Hg(NO_3)_2{\cdot}H_2O$ were used as a source of metal ions and were obtained from Sigma-Aldrich.

General methods

The elemental analysis of receptor **1** was acquired on the Exeter Analytical Inc. model CE-440 CHN analyzer. FT-IR spectral analysis was obtained from a Shimadzu FT-IR spectrometer using KBr pallets (4000–400 cm^{-1}), and electronic absorption spectra were procured from a Systronics double-beam UV-vis spectrophotometer (2201). ^1H (500 MHz) and ^{13}C (500 MHz) were obtained from Bruker and Jeol Delta-2 spectrometers, respectively, using DMSO-d_6 as solvent and tetramethylsilane (TMS) as internal reference material. NMR chemical shift values are mentioned in parts per million (ppm). Fluorescence spectra were recorded on the fluorescence spectrophotometer RF-5301. Electrospray ionization-high-resolution mass spectra (ESI-HRMS) were obtained from a MICROMASS QUATTRO II triple quadrupole mass spectrometer. The ESI capillary was set at 3.5 kV, and the cone voltage was 40 V. Electrochemical measurements were recorded on NOVA version 1.10.1.9 Metrohm Autolab PGSTAT128 comprising glassy carbon electrode (GCE) as working electrode, Ag/AgCl (saturated KCl) as reference electrode and a platinum wire as counter electrode.

Synthesis of 2-(4-(diethylamino)-2-hydroxyphenyl)-1*H*-anthra[1,2-*d*]imidazole-6,11-dione (1)

To a stirring solution of 1,2-diaminoanthraquinone (0.23 g, 1.0 mmol) in nitrobenzene (5 mL) was added 4-diethylaminosalicylaldehyde (0.20 g, 1.0 mmol) in nitrobenzene (5 mL). The resulting solution was refluxed at 140 °C for 16 h as the progress of reaction was monitored by TLC. The reaction mixture was then cooled to rt, and the product was precipitated by slow addition of diethyl ether (25 mL) to the reaction mixture. Dark pink precipitate of the desired compound thus obtained was washed with diethyl ether (3 × 8 mL) and dried *in vacuo*. The product nature was completely non-crystalline, and various types of attempts (solvent combinations) were made to get single crystals. Finally, crystals suitable for single-crystal X-ray diffraction analysis were obtained by vapor diffusion method by filing the inner tube with a dichloromethane solution of **1**, and the outer tube with 1 : 1 (v/v) diethyl ether/PET ether (40–60). Yield = 84% (0.346 g). Analytical data: anal. calc. for $C_{25}H_{21}N_3O_3$ (411.16): C, 72.98; H, 5.14; N, 10.21; O, 11.67; found: C, 72.94; H, 5.14; N, 10.18. FT-IR (KBr; cm^{-1}): 3435(m), 2955 (m), 2925 (w), 1664 (vs), 1632 (s), 1585 (m), 1489 (vs), 1325 (s), 1291 (vs), 1140 (m), 842 (m), 718 (vs). ^1H NMR ($CDCl_3$, 500 MHz, δ_H, ppm): 12.47 (s, 1H), 11.82 (s, 1H), 8.23 (m, 2H), 8.02 (d, 1H, J = 11.0 Hz), 7.96 (m, 2H), 6.79 (d, 2H, J = 7.5), 6.41 (d, 1H, J = 7.0 Hz), 6.34 (s, 1H), 3.41 (q, 4H), 1.16 (t, 3H). ^{13}C NMR ($CDCl_3$, 125 MHz, δ_C, ppm): 182.1, 156.1, 153.0, 150.9, 142.2, 133.7, 133.5, 132.0, 129.5, 129.0, 126.5, 126.2, 125.1, 118.5, 107.6, 105.0, 99.2, 47.2, 12.9. ESI-MS (m/z) for $C_{25}H_{21}N_3O_3$: $[M + H]^+$ calcd. 412.1583; found 412.1662 (Scheme 1).

UV-vis and fluorescence studies

To perform the absorption and emission spectral studies, 10 μM stock solution of **1** was prepared in H_2O/EtOH (7 : 3, v/v) media. Solutions of metal ions, namely, Li^+, Na^+, K^+, Mg^{2+}, Ca^{2+}, Fe^{2+}, Fe^{3+}, Co^{2+}, Ni^{2+}, Cu^{2+}, Zn^{2+}, Cd^{2+}, Hg^{2+}, Ag^+ and Pb^{2+}, of concentration 100 mM (for individual addition) and 10 mM (for titration experiments) were prepared from their nitrate salts in double distilled water, and their stock solutions were used as a source of metal ions. A 2.5 mL solution of **1** was taken in a quartz cell with 1 cm optical path length. The fluorescence experiments at rt were recorded with excitation (λ_{ex}) of **1** at 480 nm. In a typical titration, metal ions in fixed fractions were gradually added with the help of micropipette to a solution of **1**, followed by thorough mixing.

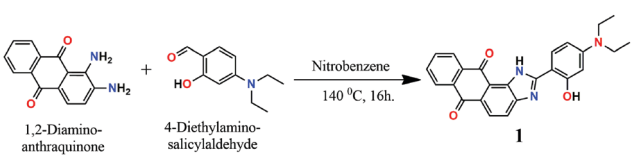

Scheme 1 Synthesis of receptor **1**.

Electrochemical studies

Redox properties of **1** were investigated on a software-aided NOVA version 1.10.1.9 Metrohm Autolab PGSTAT128N equipped with a conventional three-electrode assembly comprising glassy carbon electrode (GCE) as working electrode, Ag/AgCl (saturated KCl) as reference electrode and a platinum wire as counter electrode. Cyclic voltammetric (CV) studies were performed in H_2O/EtOH (7 : 3, v/v, 100 μM) containing 0.1 M KCl (supporting electrolyte) in the potential range of +2.0 to −2.0 V. A suitable aliquot of **1** (5 mL) was placed in an electrochemical cell, and voltammograms were recorded. To investigate the changes in ligand voltammogram, 100 mM metal ions (Li^+, Na^+, K^+, Mg^{2+}, Ca^{2+}, Fe^{2+}, Fe^{3+}, Co^{2+}, Ni^{2+}, Cu^{2+}, Zn^{2+}, Cd^{2+}, Hg^{2+}, Ag^+ and Pb^{2+}) were gradually added in fixed amounts using a micropipette. After a break period of 2.0 minutes, the voltammograms were recorded in the same potential range.

Preparation of water samples for Hg^{2+} detection

Water samples from Sagar Lake (LW), bore well (BW) from Sagar civil lines, and tap/drinking water (TW/DW) from Sagar university campus were collected and processed prior to their mercury content analysis using receptor **1**. All the water samples were filtered to separate out the insoluble material. To remove the chlorine content from tap/drinking water, it was boiled for half an hour, then cooled to rt for direct mercury analysis.

^{1}H NMR titration analysis

Receptor **1** (10 mM) was dissolved in DMSO-d_6, and firstly, a blank spectrum was recorded without metal ion addition. Then, high concentrations of the metal ions (Hg^{2+} and Cu^{2+}; 100 mM) were dissolved in D_2O, and these were added to the solution of **1** for analysis.

Results and discussion

Receptor **1** was synthesized through condensation reaction between 1,2-diaminoanthraquinone and 4-diethylaminosalicylaldehyde (1 : 1) at elevated temperature under refluxing conditions using high-boiling-point nitrobenzene as solvent. The reaction required a long timescale, but the product was obtained in reasonably good yield. Receptor **1** has been characterized by satisfactory elemental analyses and spectroscopic techniques such as FT-IR, ^{1}H, ^{13}C NMR and ESI-MS. The two low-field singlets at 12.47 and 11.82 ppm in the ^{1}H NMR spectrum of **1** were assignable to anthraimidazolyl –NH and phenolic –OH protons, respectively (Fig. S1, ESI†). Further, ESI-MS of **1** exhibited a molecular ion peak at *m*/*z* 412.1664, which is also a base peak (100% abundance) of the spectrum (Fig. S3, ESI†). Eventually, the structure of **1** has been authenticated from the single-crystal X-ray diffraction analysis.

Crystal structure of 1

The single crystals were obtained using vapor diffusion method by putting a dichloromethane solution of **1** in the inner tube and diethyl ether in the outer tube. Single-crystal structure of analogous anthraimidazoledione derivatives are quite scarce, particularly in free form (without complexation with metals).[21] The structure of **1** was verified using single-crystal X-ray diffraction data, which revealed that **1** crystallized in monoclinic crystal system with *P*21/*n* space group (Fig. 2). The crystallographic parameters of **1** are given in Table 1. It comprises a couple of chelating N^O donor sites [N(3)–O(2) and N(2)–O(1)] suitable for metal ion binding. Investigation of crystal structure depicted a highly planar structure of **1**, where the anthraquinone ring and phenylimidazole rings lie in the same plane (a maximum deviation of 0.136 Å) (Fig. S4, ESI†). The clear-cut driving force causing the extremely planar structure is a couple of intramolecular H···bonding interactions between N(3)–H(3)···O(2) and O(1)–H(1)···N(2) atoms. It is essential to elaborate here the role of H···bonding interactions in the planarity of **1**. One can see that both H···bonding interactions function at opposite sides; therefore, the hydroxyphenyl ring cannot tilt at its preferred H···bonded nitrogen site. It is further evidenced by the torsion angle involving N(2)–C(11)–C(8)–C(7), 178.2°, which is very close to 180°, thereby suggesting hindered rotation about the C–C single bond and thus the highly planar structure of **1**. The H···bond distances are comparable with the N–H···O and O–H···N distances of 2.81 and 2.60 Å, respectively (Fig. 2). Obviously, the N–H···O distance is longer than that of O–H···N, which lies with D–A distance of 2.9 Å and minimum O···N distance of 2.60 Å. However, both H···bonds can be functional in controlling the planarity of **1**.

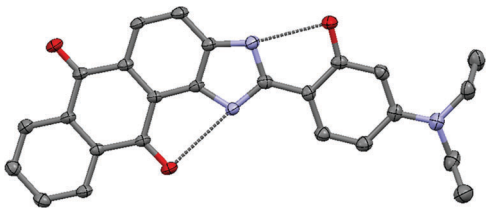

Fig. 2 Crystal structure of **1** with 50% ellipsoid probability (hydrogen atoms have been omitted for clarity).

Table 1 Crystallographic parameters of receptor **1**

Parameters	Receptor **1**
Empirical formula	$C_{25}H_{21}N_3O_3$
Crystal structure	Monoclinic
Space group	*P*21/*n*
A (Å)	7.9770(12)
B (Å)	27.642(4)
C (Å)	9.1543(13)
α (°)	90
β (°)	107.212(3)
γ (°)	90
Crystal Size (*h*, *k*, *l* max)	10 × 37 × 12
Temperature (K)	255
Volume (Å^3)	1928.1(5)
Density (g cm^{-3})	1.417
Z	4
Color and Habit	Dark pink and block
Theta(max)	28.600
*F*000	864.0
*F*000′	864.37
Absorption coefficient, *μ* (mm^{-1})	0.095

Our finding through the crystal structure of **1** is related to the similar anthraimidazole derivative, which was theoretically claimed to assume two conformational states.[22] Theoretical results suggested that conformer II, which has dual side H···bonding possibility, is less stable by 4.0 kcal than conformer I, with H···bonding at one end only. However, our results evidenced the formation of specific conformer **1**, which is structurally like the theoretically reported conformer II, having dual side H···bonding. Edge-to-edge intermolecular π–π interactions are present in **1** from both anthraquinone and hydroxyphenyl moieties (Fig. S5, ESI†). Notably, **1** extends through π–π interactions by its alternative head-to-tail and head-to-head arrangement. The bond distances and bond angles lie within the range of known analogous compounds.[23]

Absorption spectral studies

The electronic absorption spectrum of **1** displays absorption bands at 530, 335 and 266 nm (black line in Fig. 3a and Fig. S6, ESI†). The low-energy (LE) band may be ascribed to the n–π* transition, whereas the high-energy bands may be assigned to the π–π* transitions.[24] A deep pink solution of **1** motivated us to examine its colorimetric response in the presence of various metal ions under ordinary conditions (pH of **1** = 7.2 in H_2O : EtOH, 7 : 3, v/v, at rt). In this context, to a set of solutions of **1** (100 μM; 3 mL), various metal ions (10 mM) were added. Notably, clear-cut, naked-eye-visible color changes were observed from dark pink to sky blue (with Cu^{2+}) and dark yellow (with Hg^{2+}), while the rest of the tested metal ions (Na^+, K^+, Mg^{2+}, Ca^{2+}, Mn^{2+}, Fe^{2+}, Fe^{3+}, Co^{2+}, Ni^{2+}, Zn^{2+}, Ag^+, Cd^{2+} and Pb^{2+}) did not cause any colorimetric change in **1** (Fig. 3a; inset). These results reveal that **1** can be used as a naked-eye-detectable colorimetric sensor both for Cu^{2+} and Hg^{2+}. Further, electronic absorption spectra were recorded in the presence of the abovementioned cations to observe the changes. As anticipated, only Cu^{2+} and Hg^{2+} induced considerable change in the UV/vis spectra of **1** (Fig. S6, ESI†). The addition of Cu^{2+} leads to the complete disappearance of LE band at 530 nm, and a new red-shifted band appeared at 617 nm (Δ*E*, 2661 cm^{-1}). Likewise, HE band (λ_{max}, 335 nm) is red shifted (Δ*E*, 1522 cm^{-1}) to appear at 353 nm, along with a poorly structured band at 303 nm. A significant hypochromic shift was also noted in both LE (Δε, 7247 M^{-1} cm^{-1}) and HE (Δε, 8824 M^{-1} cm^{-1}) bands. The colorimetric response of **1** toward Cu^{2+} is ascribed to the red shift in LE band. In contrast, Hg^{2+} addition causes almost complete disappearance of both LE and HE bands, and the overall spectrum of **1** upon Hg^{2+} addition becomes less structured. However, after Hg^{2+} addition, the LE maximum of **1** is blue shifted (Δ*E*, 663 cm^{-1}) to appear at 512 nm, which may be responsible for the colorimetric change.

To have more precise insight on cation binding, UV/vis titration experiments were performed with Cu^{2+} and Hg^{2+} ions. The addition of a small aliquot of Cu^{2+} (2.0 μL, 0.2 equiv.) leads to a significant change in the absorption spectral feature, wherein the LE band fully disappears, along with appearance of a new red-shifted band at 617 nm, whereas the HE band (λ_{max}, 335 nm) was bathochromically shifted to appear at 353 nm (Fig. 3a and inset). Further additions of Cu^{2+} (4–20 μL) induced only subtle changes at the LE and HE bands, apart from a hyperchromic shift in the band centered at 266 nm. Notably, a new band shoulder appeared at 303 nm, whose optical density increases proportionally to the amount of added Cu^{2+}. In contrast, the addition of Hg^{2+} (2.0 μL, 0.2 equiv.) led to considerable hypochromic shift as well as blue shift (Δ*E*, 663 cm^{-1}) in the LE band to appear at 512 nm, while the HE band showed only a decrease in optical density (Δε, 7471 M^{-1} cm^{-1}) (Fig. 3b and inset). Further, gradual additions of Hg^{2+} (4.0–6.0 μL) induced concomitant hypochromic shift at 335 nm, which eventually disappeared with increased amounts of Hg^{2+} (8–20 μL). However, changes in the LE band were subtle during the increasing addition of Hg^{2+} (4–20 μL). To have better insight into the colorimetric response of **1** in the presence of Cu^{2+} and Hg^{2+} ions, the absorption spectra were carefully examined from 450–800 nm, which strongly suggested that shifts in the LE band of **1** (red shift for Cu^{2+}, blue shift for Hg^{2+} ions) are responsible for the change in color (Fig. 3, insets).

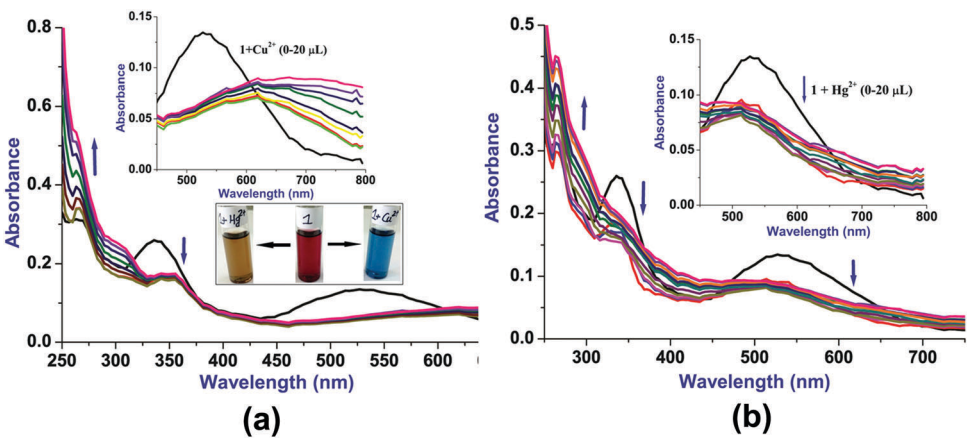

Fig. 3 UV/vis titration plots of **1** in the presence of (a) Cu^{2+} and (b) Hg^{2+} ions in H_2O/EtOH (7 : 3 v/v 10 μM) solution. Insets show the colorimetric response of **1** towards Cu^{2+} and Hg^{2+} (left, bottom), the titration plot of **1** in the presence of Cu^{2+} (left, top), and the titration plot of **1** in the presence of Hg^{2+} (right).

Furthermore, selectivity toward these cations was also investigated by the addition of Cu^{2+} (20 μL) to the solution of **1** followed by gradual addition of Hg^{2+} (2–20 μL) to the resultant **1** + Cu^{2+} solution after one hour (Fig. S6b, ESI†). Notably, the spectral pattern completely changed from **1** + Cu^{2+} to **1** + Hg^{2+}, which strongly suggested displacement of Cu^{2+} by Hg^{2+} and, thus, higher selectivity of **1** for Hg^{2+}. Job's plot analysis based on UV/vis analysis suggested a 1 : 2 binding stoichiometry between **1** and Cu^{2+} (Fig. S7, ESI†). Overall, UV/vis studies indicated the highly selective colorimetric response for Cu^{2+} and Hg^{2+} ions.

Fluorescence spectral studies

The fluorescence behavior of **1** was examined upon excitation both at its LE (530 nm) and HE (335 nm) bands, which exhibited a weak broad emission band at ~561 nm. After optimization at various wavelengths, the best-suited excitation wavelength (λ_{ex}) observed was 480 nm, which comes under the area of the broad LE absorption band. Upon excitation at 480 nm, **1** exhibited stronger emission maximum (λ_{max}) at 561 nm, and the quantum yield (Φ_F) was determined to be 0.48. The moderate Φ_F for **1** may be attributed to the high intensity of the LE absorption band. It is worth mentioning here that despite the presence of redox-active groups and extended conjugation in anthraimidazoledione derivatives, mostly their colorimetric behavior has been explored,[21,24] but redox and fluorescence response toward cations are rarely investigated.[25] Therefore, metal-ion interaction behavior of **1** was also investigated by fluorescence spectral technique, wherein different metal ions (10 equiv.; 100 mM) were separately added to the solution of **1**. Notably, none of the metal ions could cause significant fluorescence change except Hg^{2+}, which led to the large fluorescence quenching (~82%) without any wavelength shift (Fig. 4a). This suggests that the extended conjugation and planarity are not affected enough to cause any wavelength shift; thus, Hg^{2+} most probably binds with the open N^O donor site(s) of **1**. Notably, the addition of Cu^{2+} also induced a small fluorescence quenching (25.66%) without any considerable wavelength shift. This observed change has been, however, ignored for any further studies, since the changes are very similar to that of Hg^{2+} but less prominent in terms of the extent of quenching (Fig. 4a).

The fluorescence titration experiments were performed only with Hg^{2+} to gain deeper insight into the binding between **1** and Hg^{2+}. The first aliquot addition of Hg^{2+} (2.0 μL) induced a small fluorescence 'turn-off' response (8.0%) without any wavelength shift. Further addition of Hg^{2+} (5.0 μL) caused ~31% quenching with small blue-shifted fluorescence maxima (λ_{max}) at 558 nm (Fig. 4b). Increasing the concentration of Hg^{2+} (12.0 μL) added to the solution of **1** leads to large fluorescence quenching (50.0%) with a small, red-shifted maxima (λ_{max}) at 564 nm. This blue-shifted, followed by red-shifted, emission maxima with increasing amounts of Hg^{2+} (2.0–12.0 μL) added to **1**, attracted us to examine further changes by adding more Hg^{2+}. Interestingly, additions of Hg^{2+} (12–20 μL) to the solution of **1** caused great fluorescence quenching (83.0%) and the emission maxima at this stage is exactly the same as for free receptor **1**. Therefore, it is assumed that slightly blue-shifted quenched fluorescence may be attributed to the binding of Hg^{2+} through one binding site of **1**, which can cause partial loss of planarity of the receptor. In contrast, subtle red-shifted quenched maxima may be ascribed to the competitive binding of Hg^{2+} through both binding sites of **1**. This is eventually established by the revival of emission wavelength maxima (but not intensity) upon complete binding of Hg^{2+} with **1** through both binding sites, which reinstates a planar structure.

To have a better idea on the probe–metal ion binding stoichiometry, Job's plot analysis was performed, which revealed 1 : 2 stoichiometry between **1** and Hg^{2+} (Fig. S7b, ESI†). The quenching constant (K_{sv}) has been found to be 1.27×10^4 M^{-1}, derived from the Stern–Volmer plot (Fig. S8, ESI†). The association constants (K_a) for **1** + Hg^{2+} were calculated using the Benesi–Hildebrand method and found to be 1.67×10^7 M^{-1} (Fig. S9, ESI†). Furthermore, the fluorescent detection of HTM cannot be claimed unless interference of other competitors are investigated. In this context, two types of interference sequences were adopted: first, various metal cations were sequentially added to the solution containing **1** + Hg^{2+} saturated complex; second, Hg^{2+} was added separately into the solution containing **1** + M^{n+} (M = various tested cations; Fig. S10, ESI†). Notably, none of the metal ions interfere significantly with the **1** + Hg^{2+} complex, which suggests the high selectivity of **1** toward Hg^{2+}.

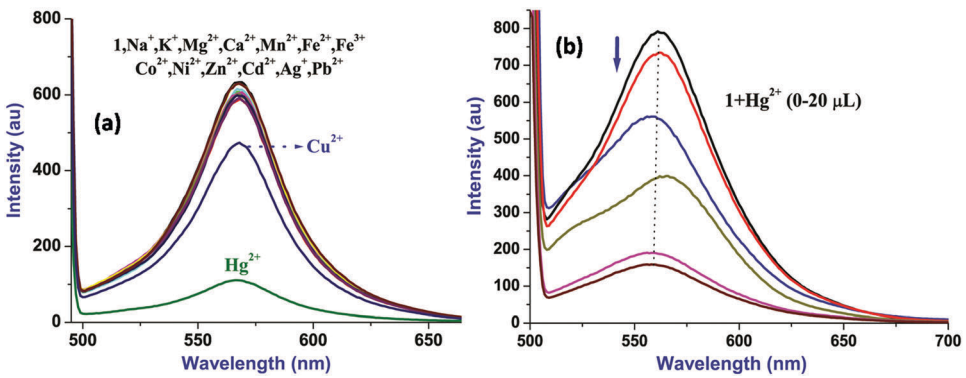

Fig. 4 (a) Fluorescence spectra of **1** (10 μM) in the presence of 10 equiv. of various metal ions in H_2O/EtOH (7 : 3 v/v); (b) fluorescence titration plots of **1** in the presence of Hg^{2+} ions in H_2O/EtOH (7 : 3, v/v; 10 μM) solution.

To measure the sensitivity of the receptor toward Hg^{2+}, varying concentrations of Hg^{2+} (10^{-15}–10^{-6} M) were added to the solutions containing **1** (1.0 μM) (Fig. S11, ESI†). A plot of fluorescence intensity *vs.* concentration displayed significant change at very low concentration (10^{-15} M) for Hg^{2+}, which indicated the femtomolar-level sensitivity of **1** toward Hg^{2+} (Fig. S11a, ESI†). However, the addition of 1.0×10^{-15} to 9.0×10^{-15} M concentrations could not give a linear quenching response. Therefore, to *g* better accuracy, 10^{-12} M solutions of Hg^{2+} (1.0×10^{-12} to 9.0×10^{-12} M) were added to the solution of **1** (1.0 μM). A plot between fluorescence intensity (F_0/F) and Hg^{2+} concentration showed a linear relationship ($R^2 = 0.99$) and indicated a limit of detection (LOD) of 1.0×10^{-12} M (Fig. S11b, ESI†). It strongly suggested that receptor **1** can be potentially used for the practical detection of Hg^{2+}. The reversibility of the receptor was verified by adding excess EDTA (5.0 equivalent with respect to **1**), which almost completely restored the fluorescence due to **1**. Further, the pure receptor **1** was extracted with dichloromethane, then air dried and reused for Hg^{2+} detection. To our delight, when used for the second time, receptor **1's** performance is identical to that of pure **1**, which suggests its reusability without decrease in the Hg^{2+} detection performance. However, its reusability was not tested more than twice, but it is worth mentioning that **1** is highly stable at elevated temperature, as it was synthesized at 130 °C, and it is unaffected by any solvent system, as evident from performing experiments in aqueous medium and NMR spectrum in DMSO.

Practical identification of Hg^{2+} in various real water samples

The highly sensitive and selective fluorescent detection of Hg^{2+} using receptor **1** without interference from other competitive cations encouraged us to apply **1** for the practical determination of trace Hg^{2+} in real water samples from various sources. As mentioned earlier, stock solutions of the collected water samples were well prepared before analysis. Initially, the fluorescence spectrum was recorded after taking 2.5 mL of distilled water in a quartz cuvette and adding 250 μL of **1** (100 μM; H_2O–EtOH, 7 : 3, v/v) into it. Likewise, pretreated water samples from tap water (TW), bore well water (BW) and lake water (LW) sources were separately taken in a quartz cuvette, and 250 μL of **1** (100 μM) was added to them. Notably, small fluorescence quenching (13–20%) was observed in these drinking water samples; however, the lake water showed optimum quenching of fluorescence (~20%) (Fig. 5a). Further, we manually added 20 μL of Hg^{2+} (10^{-9} M) to the **1** + LW solution (250 μL + 2.5 mL), which led to a large fluorescence quenching (~42.0%).

To check the linearity of the response of **1** toward real water samples, we added 100–500 μL of real water samples to the solution of **1** (2.5 mL; 10 μM), which led to a very small quenching of the fluorescence, but in good linearity (Fig. 5b). The mixture of real water samples and **1** were kept for 24 h and thereafter analyzed again by fluorescence spectroscopy, which showed an exact overlapping with the spectra obtained just after two minutes, strongly suggesting the ultra-sensitivity of **1** toward Hg^{2+} ion. The results obtained from analyzing real water samples strongly recommended **1** to be used as a potential fluorescent receptor for the practical detection of Hg^{2+} in competitive environment as well as its possible uses for other environmental and biomedical applications. Based on the significant quenching in **1** upon addition of 20 μL ppb concentration (~0.2 ppb), it is evident that the lake water contains Hg^{2+} (<0.2 ppb) at the present stage. However, lake water comprises the maximum concentration compared with university drinking tap water and city bore well water. Overall, this sensor works well and is synthesized through an easy single step; the chemicals required are easily available, and the detection of Hg^{2+} through fluorescence technique is facile.

Electrochemical studies

The presence of the redox-active anthraquinone group in **1** prompted us to explore the electrochemical behavior of receptor **1** (100 μM) in the potential range of −2.0 to +2.0 V. Therefore, cyclic voltammetry (CV) experiments were performed in H_2O–EtOH (7 : 3, v/v) media using 0.1 M KCl as a supporting electrolyte at a scan rate of 0.1 V s^{-1}. The cyclic voltammogram of **1** exhibits an irreversible single reductive wave, −0.59 V, assignable to the reduction of anthraquinone moiety (Fig. 6 and Fig. S12, ESI†).[26] However, **1** does not show any oxidative wave, which may be attributed to the presence of the ketonic form of the anthraimidazole moiety.

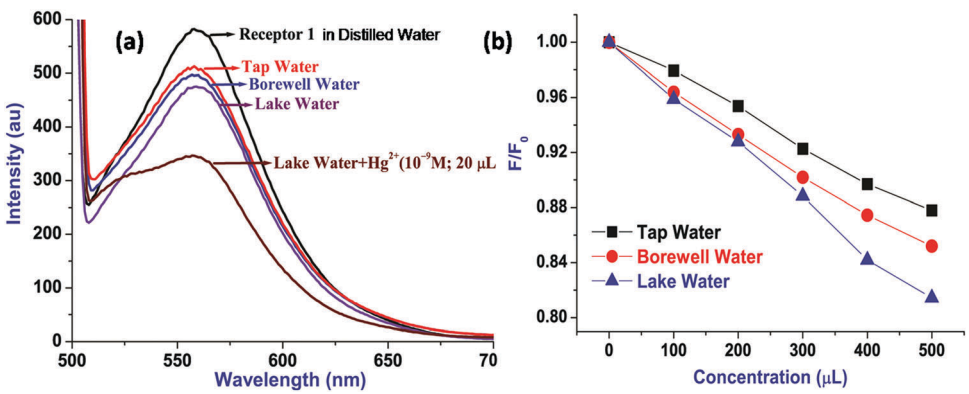

Fig. 5 (a) Fluorescence response of **1** towards Hg^{2+} determination in real water samples from different sources and upon manual ppb level addition of Hg^{2+} (20 μL) to the lake water. (b) Linear fluorescence quenching response of **1** towards real water samples.

The metal ion binding properties of **1** were also probed through electrochemical responses under analogous conditions. As KCl was used as a supporting electrolyte and considering negligible changes caused by alkali and alkaline earth metal ions in UV/vis and fluorescence studies, we have omitted these cations from electrochemical studies for better clarity. The addition of 100 mM other cations (Mn^{2+}, Fe^{2+}, Fe^{3+}, Co^{2+}, Ni^{2+}, Cu^{2+}, Zn^{2+}, Cd^{2+}, Hg^{2+}, Ag^{+} and Pb^{2+}) to the solution of **1** (100 μM) induced insignificant changes to the electrochemical features of **1**, except for Cu^{2+} (causes significant changes only in current intensity) and Hg^{2+} (leads to the appearance of a new reversible oxidative wave) (Fig. S12, ESI†). Therefore, electrochemical (CV) titration experiments were performed in the presence of Cu^{2+} and Hg^{2+}. Gradual addition of Cu^{2+} (0–50 μL) causes significant change in the current intensity (ΔI, 2.62×10^{-6}) however, no potential shift was observed (Fig. 6a).

Notably, the initial addition of Cu^{2+} (10 μL) leads to a small current intensity change (ΔI, 0.66×10^{-6}) without altering the cyclic voltammogram features, but increasing amounts (20–50 μL) changed the electrochemical features along with considerable current intensity changes (Fig. 6a). In contrast, initial Hg^{2+} addition (10 μL) induces a small current intensity change (ΔI, 0.34×10^{-6}) without any potential shift in the reductive wave (Fig. 6b). However, a new reversible oxidative wave (ΔV, 0.09) appeared at +0.11 V. Further, additions of Hg^{2+} (20–40 μL) led to an increase in the current intensities of both the reductive (ΔI, 1.17×10^{-6}) and oxidative waves (ΔI, 2.84×10^{-6}) without any additional potential shift. The appearance of a new oxidative wave at +0.11 V may be attributed to the complexation-induced chalcogen (phenolic –OH group) oxidation. It is worth mentioning that the sensitivity and selectivity of **1** has been found to be much better for Hg^{2+} relative to Cu^{2+}. Overall, the electrochemical studies suggested the detection of both Cu^{2+} and Hg^{2+}, but selectivity is best suited for Hg^{2+}, which induced the appearance of a new signal in the oxidation window (Fig. 6a).

The multichannel detection of Cu^{2+} and Hg^{2+} by **1** requires a better understanding of the binding mode of the receptor. However, in examining the structure of **1**, it is clear that both open N^O donor sites are capable of binding to these metal ions. In fact, such imidazolyl and phenolic protons generally require a base or higher temperature, and the resulting deprotonated species binds well with all the cations. Using this approach, we have successfully synthesized a series of M_2(**1**) complexes (M = Co^{2+}, Ni^{2+}, Zn^{2+} and Cd^{2+}), which are not discussed in the present work. To have better insight, ^{1}H NMR titration experiments on **1** were carried out in the presence of Hg^{2+} and Cu^{2+} in DMSO-d_6 (Fig. 7). Since NMR titration with paramagnetic Cu^{2+} (d_9) causes large broadening of spectra, we focused on NMR titration using Hg^{2+}. The addition of Hg^{2+} (0.5 equiv.) led to the quick disappearance of both the –NH and –OH protons along with a slight upfield shift in all the protons of **1**. Further addition of Hg^{2+} (1.0 equiv.) caused broadening of the signals as well as greater upfield shift in both aromatic and aliphatic protons. Eventually, 2.0 equiv. of Hg^{2+} was added to the solution of **1**, which induced further shielding of protons, both associated to the aromatic ($\Delta\delta$, 0.032–0.219 ppm) and aliphatic parts ($\Delta\delta$: 0.13 ppm, $-CH_2$; 0.06 ppm, $-CH_3$) of **1**. In general, the protons neighboring the binding site are deshielded, but in our case, shielding in all the protons resulted. This may be attributed to the binding of Hg^{2+} ions at both sides of receptor **1** (Fig. 8), which may cause additional shielding to the protons of **1**.

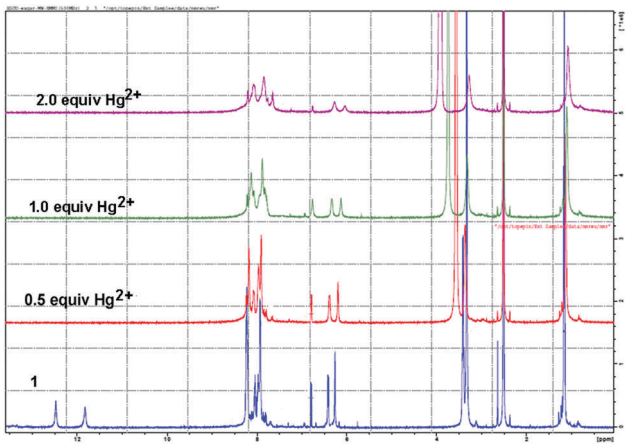

Fig. 7 ^{1}H NMR titration spectra of **1** (10 mM) in the presence of Hg^{2+} (0.5–2.0 equiv.) in DMSO-d_6.

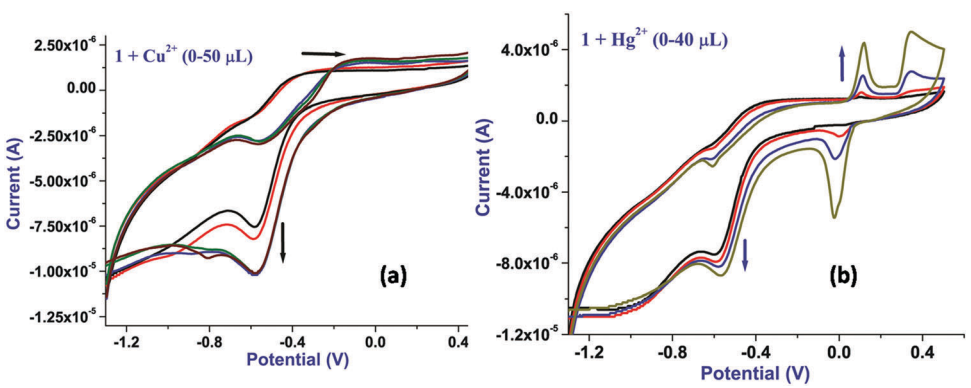

Fig. 6 Titration cyclic voltammograms of **1** (100 μM) with Cu^{2+} (a) and Hg^{2+} (b) in H_2O–EtOH (7 : 3, v/v) media using 0.1 M KCl as a supporting electrolyte.

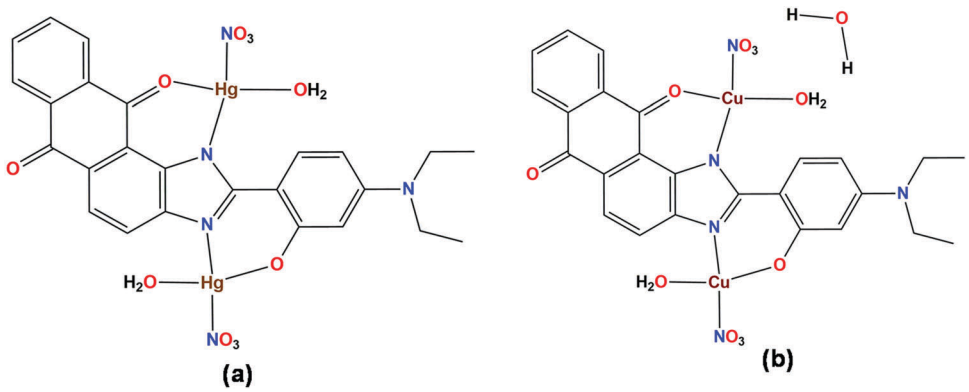

Fig. 8 Proposed molecular structures of (a) **1** + Hg^{2+} and (b) **1** + Cu^{2+} based on electronic (UV/vis, fluorescence) spectroscopy, Job's plot analysis, ^1H NMR and ESI-MS spectral techniques.

Likewise, the addition of just 0.5 equiv. of Cu^{2+} to the solution of **1** induced a large broadening, where the exact positions of protons were hard to assign; therefore, further Cu^{2+} addition was stopped (Fig. S13, ESI†). The broadening is associated with the presence of paramagnetic Cu^{2+} ions interacting with **1**. However, the ^1H NMR spectral feature in the presence of Cu^{2+} was like that observed for Hg^{2+}.

To further strengthen the structural insights, ESI-MS spectra were acquired on complexes obtained by the reactions of $Hg(NO_3)_2{\cdot}H_2O$ and $Cu(NO_3)_2{\cdot}3H_2O$ with **1** at rt in H_2O–EtOH medium. The ESI-MS spectrum of the **1** + Hg^{2+} complex displayed a clear-cut molecular ion peak at *m*/*z* 972.0778 $[M + H]^+$ corresponding to $[Hg_2(\mathbf{1})(NO_3)_2(H_2O)_2]^+$ (Fig. 8a and Fig. S14a, ESI†), along with a base peak at 412.1640 assignable to **1**. Likewise, **1** + Cu^{2+} exhibited $[M + H]^+$ peak at *m*/*z* 714.5823, which may be attributed to the $[Cu_2(\mathbf{1})(NO_3)_2(H_2O)_2]^+{\cdot}H_2O$ entity (Fig. 8b and Fig. S14b, ESI†), along with a base peak at *m*/*z* 412.1653 corresponding to **1**. Overall, based on the UV/vis, fluorescence, Job's plot analysis, ^1H NMR titration and ESI-MS spectral techniques, it has been proposed that both Cu^{2+} and Hg^{2+} bind in 1 : 2 (probe : metal) stoichiometry with **1**, as shown in Fig. 8. The binding of metal ions through doubly bonded quinone oxygen is also known.[24c]

Conclusion

In summary, we have developed a highly reusable, simplistic, selective and sensitive anthraimidazoledione-based multichannel receptor **1** for the recognition of biologically and environmentally important Cu^{2+} and Hg^{2+} ions. The crystal structure of **1** has been developed, which is rarely known for non-complexed anthraimidazoledione derivatives. The receptor detects Cu^{2+} through a naked-eye-detectable colorimetric change and quantitatively recognizes Hg^{2+} through colorimetric change as well as large fluorescence quenching as a detection response in the background presence of other competing HTMs, including Cu^{2+}. Furthermore, interactions of **1** with Cu^{2+} and Hg^{2+} were also detected through electrochemical changes, both in potential shift and current intensity. Receptor **1** displays efficiency in detecting both Cu^{2+} and Hg^{2+} through colorimetric, fluorimetric and electrochemical responses. The probe–metal ion binding has been examined and supported by UV/vis, fluorescence, ^1H NMR titration and ESI-MS spectral techniques. Eventually, **1** was successfully used as a highly selective and ultrasensitive receptor for the practical detection of trace-level Hg^{2+} in real water samples, where lake water contained the maximum concentration of Hg^{2+} detected but was <0.2 ppb.

Conflicts of interest

There are no conflicts to declare.

Acknowledgements

MAW is thankful to UGC for providing financial assistance and to the Department of Chemistry, Dr H. S. Gour Central University Sagar, (MP) India, for providing the necessary facilities. MDP is thankful to the university grants commission for the UGC-startup grant [F. No. 30-56/2014(BSR)] and DST India for SERB research grant (EMR/2016/001779). RP acknowledges DST for providing financial assistance through DST-Inspire Faculty scheme (IFA12-CH-66).

References

1 (*a*) F. Zapata, A. Caballero, A. Espinosa, A. Tárraga and P. Molina, *J. Org. Chem.*, 2009, **74**, 4787–4796; (*b*) H. Yang, Z. Zhou, K. Huang, M. Yu, F. Li, T. Yi and C. Huang, *Org. Lett.*, 2007, **9**, 2729–2732; (*c*) F. Sancenon, R. Martinez-Manez, M. A. Miranda, M. J. Segui and J. Soto, *Angew. Chem., Int. Ed.*, 2003, **42**, 647–650; (*d*) D. Mondal, P. Pal and S. Baitalik, *Sens. Actuators, B*, 2017, **242**, 746–759.

2 (*a*) A. Thakur, S. Sardar and S. Ghosh, *Inorg. Chem.*, 2011, **50**, 7066–7073; (*b*) C. Arivazhagan, R. Borthakur and S. Ghosh, *Organometallics*, 2015, **34**, 1147–1155; (*c*) M. Schmittel and H. W. Lin, *Angew. Chem., Int. Ed.*, 2007, **46**, 893–896.

3 L. Amin-Zaki, S. Elhassani, M. A. Majeed, T. W. Clarkson, R. A. Doherty and M. Greenwood, *Pediatrics*, 1974, **54**(5), 587–595.

4 W. F. Fitzgerald, D. R. Engstrom, R. P. Mason and E. A. Nater, *Environ. Sci. Technol.*, 1998, **32**, 1–7.

5 E. M. Nolan and S. J. Lippard, *Chem. Rev.*, 2008, **108**, 3443–3480.

6 (*a*) World Health Organization, Guidelines for Drinking-water Quality, Incorporating First Addendum. vol. 1, Recommendations, 3rd edn, 2006; (*b*) Background on Drinking Water Standards in the Safe Drinking Water Act (SDWA), https://www.epa.gov/-dwstandardsregulations/background-drinking-water-standards-safe-drinking-water-act-sdwa; (*c*) C. W. C. Leong, I. N. Syed and L. F. Lorscheider, *Neuroreport*, 2001, **12**, 733–737.

7 (*a*) W. Shu, L. Yan, J. Liu, Z. Wang, S. Zhang, C. Tang, C. Liu, B. Zhu and B. Du, *Ind. Eng. Chem. Res.*, 2015, **54**, 8056–8062; (*b*) N. Kaur, G. Dhaka and J. Singh, *New J. Chem.*, 2015, **39**, 6125–6129; (*c*) Y.-M. Zhang, K.-P. Zhong, J.-X. Su, X.-P. Chen, H. Yao, T.-B. Wei and Q. Lin, *New J. Chem.*, 2017, **41**, 3303–3307.

8 R. Uauy, M. Olivares and M. Gonzalez, *Am. J. Clin. Nutr.*, 1998, **67**, 952S–959S.

9 M. C. Linder and M. Hazegh-Azam, *Am. J. Clin. Nutr.*, 1996, **63**, 797S–811S.

10 P. G. Georgopoulos, A. Roy, M. J. Yonone-Lioy, R. E. Opiekun and P. J. Lioy, *J. Toxicol. Environ. Health, Part B*, 2001, **4**, 341–394.

11 A. Anandhan, H. Rodriguez-Rocha, I. Bohovych, A. M. Griggs, L. Zavala-Flores, E. M. Reyes-Reyes, J. Seravalli, L. A. Stanciu, J. Lee, J. C. Rochet, O. Khalimonchuk and R. Franco, *Neurobiol. Dis.*, 2015, **81**, 76–92.

12 X. Dai, F. Qiu, X. Zhou, Y. Long, W. Li and Y. Tu, *Anal. Chim. Acta*, 2014, **848**, 25–31.

13 L. M. Gaetke and C. K. Chow, *Toxicology*, 2003, **189**, 147–163.

14 Z. Guo, G. Chen, G. Zeng, Z. Li, A. Chen, M. Yan, L. Liu and D. Huang, *RSC Adv.*, 2014, **4**, 59275–59283.

15 M. D. Tutulea-Anastasiu, D. Wilson, M. del Valle, C. M. Schreiner and I. Cretescu, A Solid-Contact Ion Selective Electrode for Copper(II) Using a Succinimide Derivativeas Ionophore, *Sensors*, 2013, **13**, 4367–4377.

16 A. Thakur and S. G. Ghosh, *Organometallics*, 2012, **31**, 819–826.

17 (*a*) M. A. Wani, P. K. Singh, R. Pandey and M. D. Pandey, *J. Lumin.*, 2016, **171**, 159–165; (*b*) R. Pandey, P. Kumar, A. K. Singh, M. Shahid, P. Li, S. K. Singh, Q. Xu and A. Misra, *Inorg. Chem.*, 2011, **50**, 3189–3197; (*c*) R. Pandey, R. K. Gupta, M. Shahid, B. Maiti, A. Misra and D. S. Pandey, *Inorg. Chem.*, 2011, **51**, 298–311; (*d*) A. Kumar, R. Pandey, A. Kumar and D. S. Pandey, *RSC Adv.*, 2014, **4**, 55967–55970; (*e*) R. Pandey, M. Yadav, M. Shahid, A. Misra and D. S. Pandey, *Tetrahedron Lett.*, 2012, **53**, 3550–3555; (*f*) A. Kumar, M. Dubey, R. Pandey, R. K. Gupta, A. Kumar, A. C. Kalita and D. S. Pandey, *Inorg. Chem.*, 2014, **53**, 4944–4955; (*g*) S. Mukhopadhyay, A. Biswas, R. Pandey, R. K. Gupta and D. S. Pandey, *Tetrahedron Lett.*, 2014, **55**, 1437–1440; (*h*) A. Biswas, R. Pandey, D. Kushwaha, M. Shahid, V. K. Tiwari and A. Misra, *Tetrahedron Lett.*, 2013, **54**, 4193–4197.

18 (*a*) A. Helal, H. S. Kim, Z. H. Yamani and M. N. Shaikh, *J. Fluoresc.*, 2016, **26**, 1–9; (*b*) N. Kaur and P. Alreja, *J. Chem. Sci.*, 2015, **127**, 1253–1259.

19 S. H. Choi, K. Pang, K. Kim and D. G. Churchill, *Inorg. Chem.*, 2007, **46**, 10564–10577.

20 D. D. Perrin, W. L. F. Armango and D. R. Perrin, *Purification of laboratory Chemicals*, *Pergamon*, Oxford, UK, 1986.

21 (*a*) B. Bhattacharyya, A. Kundu, A. Das, K. Dhara and N. Guchhait, *RSC Adv.*, 2016, **6**, 21907–21916; (*b*) D. Mondal and S. Baitalik, *ChemistrySelect*, 2016, **1**, 1318–1328; (*c*) A. J. Hallett, B. D. Ward, B. M. Kariuki and S. J. A. Pope, *J. Organomet. Chem.*, 2010, **695**, 2401–2409.

22 V. Luxami and S. Kumar, *Dalton Trans.*, 2012, **41**, 4588–4593.

23 R. Pandey and D. S. Pandey, *J. Indian Chem. Soc.*, 2012, **89**, 1123–1134.

24 (*a*) A. Sarkar, S. Bhattacharya and A. Mukherjee, *Dalton Trans.*, 2016, **45**, 1166–1175; (*b*) N. Kumari, S. Jha and S. Bhattacharya, *J. Org. Chem.*, 2011, **76**, 8215–8222; (*c*) C. Marín-Hernandez, L. E. Santos-Figueroa, M. E. Moragues, M. M. M. Raposo, R. M. F. Batista, S. P. G. Costa, T. Pardo, R. Martínez-Manez and F. Sancenon, *J. Org. Chem.*, 2014, **79**, 10752–10761; (*d*) S. R. Bobe, S. V. Bhosale, L. Jones, A. L. Puyad, A. M. Raynor and S. V. Bhosal, *Tetrahedron Lett.*, 2015, **56**, 4762–4766; (*e*) A. Ghosh, D. A. Jose and R. Kaushik, *Sens. Actuators, B*, 2016, **229**, 545–560; (*f*) R. M. F. Batista, E. Oliveira, S. P. G. Costa, C. Lodeiro and M. M. M. Raposo, *Supramol. Chem.*, 2014, **26**, 71–80.

25 (*a*) R. M. F. Batista, E. Oliveira, S. P. G. Costa, C. Lodeiro and M. M. M. Raposo, *Org. Lett.*, 2007, **9**, 3201–3204; (*b*) D. Mondal, M. Bar, D. Maity and S. Baitalik, *J. Phys. Chem. C*, 2015, **119**, 25429–25441; (*c*) B. Bhattacharyya, A. Kundu, N. Guchhait and K. Dhara, *J. Fluoresc.*, 2017, **27**, 1041–1049; (*d*) R. M. F. Batista, S. P. G. Costa and M. M. M. Raposo, *J. Photochem. Photobiol., A*, 2013, **259**, 33–40.

26 (*a*) D. Mondal, M. Bar, S. Mukherjee and S. Baitalik, *Inorg. Chem.*, 2016, **55**, 9707–9724; (*b*) C. J. da Cunha, E. S. Dodsworth, M. A. Monteiro and A. B. P. Lever, *Inorg. Chem.*, 1999, **38**, 5399–5409.

